Catalysis Today 146 (2009) 25–30

Contents lists available at ScienceDirect

Catalysis Today

journal homepage: www.elsevier.com/locate/cattod

Hollow spherical carbon with mesoporous shell as a superb anode catalyst support in proton exchange membrane fuel cell

Jung Ho Kim, Baizeng Fang, Minwoo Kim, Jong-Sung Yu *

Department of Advanced Materials Chemistry, BK21 Research Team, Korea University, 208 Seochang, Jochiwon, ChungNam 339-700, Republic of Korea

ARTICLE INFO

Article history:
Available online 20 March 2009

Keywords:
Hollow core mesoporous shell carbon
Electrocatalyst
Catalyst support
Hydrogen oxidation
Proton exchange membrane fuel cell

ABSTRACT

Hollow core mesoporous shell carbon (HCMSC) has been explored for the first time as an anode catalyst support in proton exchange membrane fuel cell (PEMFC). The fantastic structural characteristics of the HCMSC such as large specific surface area and mesoporous volume and well-developed three-dimensionally interconnected bimodal porosity make it an excellent catalyst support in PEMFC. The supported PtRu nanoparticles have shown smaller particle size and better dispersion on the HCMSC than on commercial carbon black Vulcan XC-72. Considerable improvements in the electrocatalytic activity toward H_2 oxidation and fuel cell performance have been demonstrated by the HCMSC-supported PtRu nanoparticles compared with Vulcan XC-72 supported ones (i.e., corresponding to an enhancement of more than 60% in power density compared with that of PtRu/Vulcan), implying that HCMSC is a superb anode catalyst support in PEMFC.

1. Introduction

Proton exchange membrane fuel cell (PEMFC) has demonstrated great promise as a future energy source for portable applications such as electric vehicles and small portable electronics, and stationary applications including distributed home power generators [1,2]. However, commercialization of the PEMFC technology is hindered by the high cost of Pt, which is the dominant electrocatalytic element both in anode and cathode catalyst layers. In addition, Pt is also susceptible to CO poisoning [3,4]. Much effort has been made to lower Pt usage and/or improve its CO-tolerance. One of effective approaches is alloying of Pt with transition metals such as Fe, Co, Ni, Sn [5,6], Bi, In, Pb, Cu [7,8] or with less expensive noble metals such as Ir [9,10], Ru [11–13], Au [14], Pd [15] or using non-Pt-based metal or alloy such as Pd [15], Pd–Co [16], Pd–Co–Au [17]. So far, Ru has been proved as one of the most widely investigated promoters in Pt-based anode catalysts for low temperature fuel cells.

Catalyst support technology has been also proved as effective strategy to lower Pt usage and enhance CO-tolerance of the supported catalyst. Carbon is one of the most promising catalyst support candidates, which has attractive characteristics such as high inertness under harsh chemical and electrochemical conditions, high surface area and electrical conductivity, well-developed porosity, adequate water-handling capability and low cost. Carbon black Vulcan XC-72 (VC) has been frequently used as a catalyst support in low temperature fuel cells. However, the VC contains large quantity of primary micropores of less than 1 nm in diameter, and many Pt nanoparticles trapped in the micropores were not involved in the electrochemical reactions on electrodes due to the absence of the triple-phase boundaries. Various novel carbon materials have been investigated as catalyst support, such as carbon nanotubes [18,19], graphitic carbon nanofibers [20], mesostructured carbon materials [21–26], macroporous carbons [27–29], and carbon microbeads [30]. These carbon-supported catalysts have shown enhanced catalytic activity toward methanol oxidation in direct methanol fuel cell (DMFC) than VC-supported one. In addition to porous carbon materials, other catalyst supports investigated include C_3N_4 [31] and WC [32,33]. They also show considerable enhancement in catalytic activity toward methanol oxidation [31,32] and hydrogen electro-oxidation [33].

Although much attention has been paid to the anode catalyst support in DMFC, little study on anode catalyst support in PEMFC has been reported. In this study, hollow core mesoporous shell carbon (HCMSC) has been investigated as an anode catalyst support in PEMFC. The HCMSC has fantastic structural characteristics such as large specific surface area and mesoporous volume, well-developed three-dimensionally interconnected bimodal porosity composed of hollow macroporous core and mesoporous shell, uniform particle size, and narrow pore size distribution (PSD) [34], which seems to be an ideal catalyst support in low-temperature

* Corresponding author. Tel.: +82 41 860 1494; fax: +82 41 867 5396.
E-mail address: jsyu212@korea.ac.kr (J.-S. Yu).

0920-5861/$ – see front matter © 2009 Elsevier B.V. All rights reserved.
doi:10.1016/j.cattod.2009.02.013

fuel cells. Our previous study had demonstrated that much higher electrocatalytic activity toward oxidation of methanol could be achieved by the HCMSC-supported $Pt_{50}Ru_{50}$ in DMFC than the commercial VC-supported one [35]. Although there are some similarities in anodic oxidation behaviour between DMFC and PEMFC anodes, large difference may exist between the catalytic activity toward methanol and hydrogen electro-oxidation even if the same anode catalyst support is used in DMFC and PEMFC. Therefore, it is necessary and significant to examine catalytic activity of the HCMSC-supported PtRu anode catalyst in PEMFC. In this study, we synthesized the HCMSC with varied core–shell structure and porosity different from that presented in previous study [35] through careful monitoring of the size of the silica spheres and the amount and ratio of tetraethoxysilane (TEOS) and octadecyltrimethoxysilane (C_{18}-TMS) added. A considerable improvement in electrocatalytic activity toward hydrogen oxidation has been accomplished by PtRu (20 wt%) supported on the HCMSC compared with its counterpart PtRu (20 wt%) supported on the VC.

2. Experimental

2.1. Preparation of HCMSC and HCSMC-supported PtRu catalyst

The HCMSC was synthesized by replication through nanocasting of solid core/mesoporous shell (SCMS) silica [34]. A typical synthesis route for SCMS silica is as follows. 40 mL of aqueous ammonia (28 wt%) was mixed with 1 L of ethanol and 80 mL of deionized water. After stirring for ca. 15 min, 60 mL of TEOS (98%, ACROS) was added, and the reaction mixture was stirred for ca. 6 h to yield uniform silica spheres (Stöber silica solution). A mixture solution containing 35.5 mL of TEOS and 14.5 mL of C_{18}-TMS (90% tech., Aldrich) was added to the colloidal solution containing the silica spheres and further reacted for 6 h. The resulting octadecyl group-incorporated silica shell/solid core nanocomposite spheres were retrieved by centrifugation, dried at room temperature and further calcined at 823 K for 6 h under an oxygen atmosphere to produce the final uniform spherical SCMS silica particles (Kaiser approach). Aluminium was incorporated into the silicate framework through an impregnation method to produce acidic points on the surface of the SCMS silica, which will catalyze polymerization of phenol and paraformaldehyde [36]. A total of 1.0 g of SCMS silica was added to an aqueous solution containing 0.27 g of $AlCl_3{\cdot}6H_2O$ in 0.3 mL of water, and the resulting slurry was stirred for 30 min. The powder was dried in air at 353 K. Finally, the Al-impregnated SCMS silica was calcined at 823 K for 5 h in air to yield SCMS aluminosilicate.

A typical synthesis route for HCMSC is as follows. 0.374 g of phenol was incorporated into the mesopores of 1.0 g of the SCMS silica template by heating at 100 °C for 12 h under vacuum. The resulting phenol-incorporated SCMS silica template was reacted with paraformaldehyde (0.238 g) under vacuum at 130 °C for 24 h to yield a phenol-resin/SCMS aluminosilicate composite. The composite was heated at 1 K/min to 160 °C and held for 5 h under a nitrogen flow. The temperature was then ramped at 5 K/min to 950 °C and held for 7 h to carbonize the cross-linked phenol resin inside the mesopores of the SCMS structure. The SCMS silica template was dissolved by using 2.0 N NaOH and the slurry washed with EtOH–H_2O solution and the as-produced HCMSC dried overnight at 80 °C.

Carbon-supported PtRu (20 wt%) catalysts were synthesized at room temperature through impregnation method using $H_2PtCl_6{\cdot}6H_2O$ (Aldrich) and $RuCl_3{\cdot}xH_2O$ (Aldrich) as metal precursors and $NaBH_4$ as a reducing agent. The catalyst inks were prepared by dispersing various carbon-supported PtRu catalysts into a mixture solution of an appropriate amount of deionized water and the required amount of 5 wt% Nafion ionomer (Aldrich). The Nafion ionomer contents in the catalyst layers were set as 20 wt%. Appropriate amounts of the catalyst inks were painted uniformly on Teflonized carbon paper (TGPH-090) and dried at 70 °C overnight.

2.2. Surface characterization of HCMSC and HCMSC-supported PtRu catalyst

N_2 adsorption and desorption isotherms were measured at 77 K on a KICT SPA-3000 Gas Adsorption Analyzer after the carbon was degassed at 423 K to 20 μTorr for 4 h. The specific surface areas were determined from nitrogen adsorption using the Brunauer–Emmett–Teller (BET) equation. The total pore volumes were determined from the amounts of gas adsorbed at the relative pressure of 0.99. Micropore (pore size <2 nm) volumes of the porous carbons were calculated from the analysis of the adsorption isotherms using the Horvath–Kawazoe (HK) method. Pore size distribution was derived from the analysis of the adsorption branch using the Barrett–Joyner–Halenda (BJH) method. Scanning electron microscopy (SEM) images were obtained using a Hitachi S-4700 microscope operated at an acceleration voltage of 10 kV. Transmission electron microscopy (TEM) was operated on EM 912 Omega at 120 kV, and high-resolution TEM (HR-TEM) images were obtained by using JEOL FE-2010 microscope operated at 200 kV. X-ray diffraction (XRD) analyses for carbon samples and the supported PtRu catalysts were carried out with a Rigaku 1200 using Cu Kα radiation and a Ni β-filter and operating at 40 kV and 20 mA.

2.3. Half-cell and single cell tests

Half cell (i.e., three-electrode electrochemical cell) tests were conducted to examine electrochemical surface areas of Pt in various carbon-supported PtRu catalysts. In all cases, Pt gauze was used as the counter electrode and Ag/AgCl as the reference one. The working electrode was a thin layer of Nafion-impregnated catalyst cast on a glassy carbon disk (3 mm in diameter) embedded in a Teflon cylinder. The catalyst layer on the working electrode was prepared as follows [37]. First, 5 mg of carbon-supported PtRu (20 wt%) catalyst was dispersed in 1 mL of solution of deionized water and ethanol with a volume ratio of 1:4. Then, 50 μL of Nafion solution (5 wt% Nafion) was added and ultrasonicated for 1 h. Next, 5 μL of the slurry was pipetted and spread on the top of a glassy carbon disk. Finally, the catalyst-coated glassy carbon electrode was dried at 70 °C for 2 h to yield a loading of 20 μg Pt/cm^2. Cyclic voltammetric (CV) measurements were conducted in 0.5 M H_2SO_4 at room temperature with a scan rate of 25 mV/s. Electrolyte solution was deaerated by high-purity nitrogen for 1 h prior to any cyclic voltammetric measurement and stable voltammograms were recorded after 10 cycles.

Single cells were constructed to evaluate catalytic activities toward H_2 oxidation and fuel cell performance of various carbon-supported $Pt_{50}Ru_{50}$ (20 wt%) anode catalysts. E-TEK VC-supported Pt (20 wt%) was used as cathode catalyst. The catalyst loadings were 0.4 mg $Pt_{50}Ru_{50}$/cm^2 at the anode and 0.2 mg Pt/cm^2 at the cathode. The membrane electrode assembly (MEA) was employed to construct a single fuel cell, which had been fabricated by hot-pressing a pretreated Nafion115 (Du-Pont) sandwiched by the anode and cathode. Performance tests of fuel cells were conducted under constant current using a unit cell with a 6.25 cm^2 cross-sectional catalyst area with a WFCTS fuel cell test station (WonA Tech Co., Ltd., Korea). After being humidified at a temperature of 15 °C higher than the cell operating temperature, H_2 and O_2 were supplied to the anode and cathode with zero back pressure at flow rates of 100 and 500 mL/min, respectively.

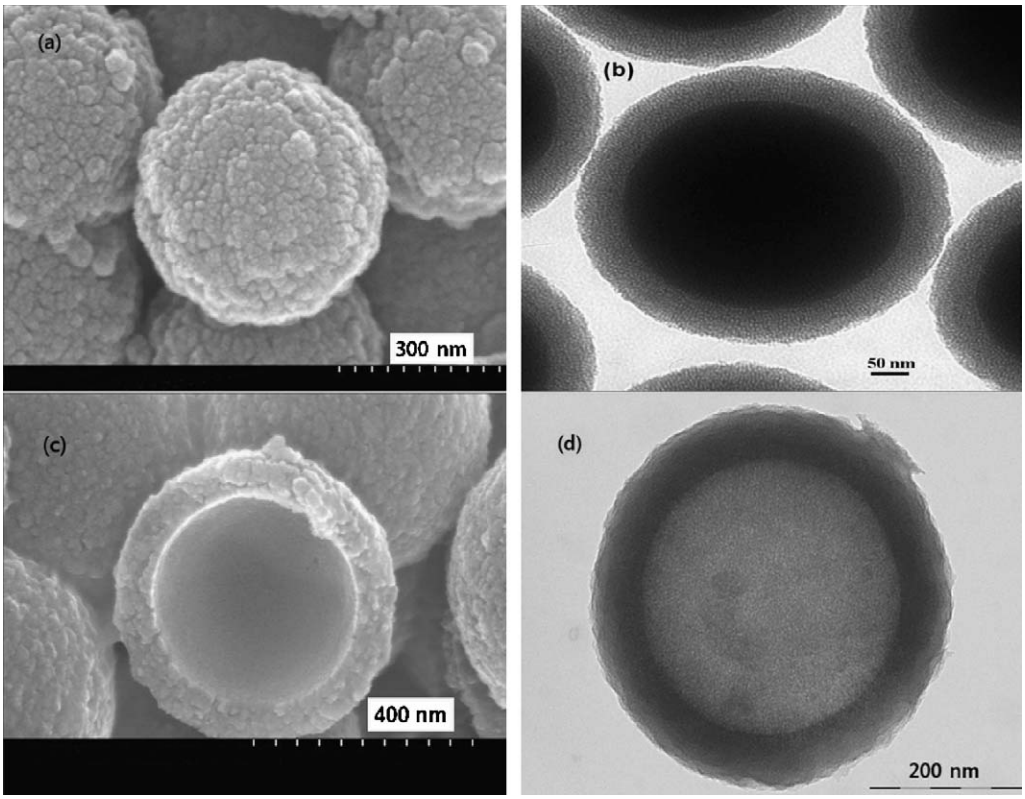

Fig. 1. Representative SEM (a) and TEM (b) images of the SCMS silica, and SEM (c) and TEM (d) images of the HCMSC replica.

3. Results and discussion

3.1. Structural characteristics of the HCMSC and carbon-supported catalysts

Fig. 1a and b shows representative SEM and TEM images of the SCMS silica, respectively. It is evident from the SEM image (Fig. 1a) that most of the SCMS silica particles are spherical and uniform with particle sizes of 490 to 510 nm (mean size of ca. 500 nm). The TEM image (Fig. 1b) shows that the SCMS silica has a solid core of ca. 370 nm in diameter and shell thickness of ca. 65 nm. In contrast, the SEM (Fig. 1c) and TEM (Fig. 1d) images of the HCMSC suggest an inverse replication of the SCMS silica, and that the HCMSC has a hollow core diameter of ca. 360 nm and shell thickness of ca. 63 nm, showing a slight shrinkage compared with those of its parent silica template. It is evident that the diameter of the hollow core and the mesoporous shell thickness of the HCMSC can be controlled independently by using appropriate SCMS silica template, which can be produced in various sizes and various shell thicknesses by using the solid silica spheres with various particle sizes and adjusting the molar ratio of C_{18}-TMS to TEOS, respectively.

Fig. 2 shows nitrogen adsorption–desorption isotherms for the HCMSC, which indicate rather complex multimodal pore size distribution. The nitrogen isotherms are type-IV typical of mesoporous material with clear capillary condensation step according to the International Union of Pure and Applied Chemistry nomenclature and suggest a narrow PSD centred at ca. 3.5 nm. Surface structural parameters for the HCMSC and VC are summarized in Table 1. The HCMSC exhibits a very large BET surface area (i.e., 1767 m^2/g) and total pore volume (i.e., 2.21 cm^3/g), which are mainly attributable to the presence of the mesopores in the shell (mesopore volume: 1.60 cm^3/g) with some micropores. Hence, each of the carbon capsules has a bimodal pore system composed of a spherical macroporous core and mesopores in the shell connecting the inside and outside of the hollow macroporous core. In contrast, the VC exhibits an appreciable amount of micropores (<2 nm) in addition to mesopores and macropores with varying sizes.

Fig. 3 shows representative TEM images for the PtRu (20 wt%) nanoparticles supported on the HCMSC (a and b) and on the VC (c and d). PtRu nanoparticles are dispersed homogenously as small, spherical and uniform dark spots over the entire surface of the HCMSC support. The size of the PtRu nanoparticles determined

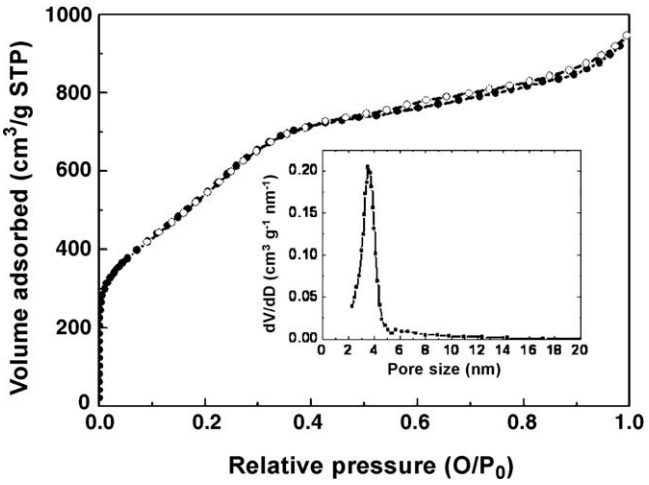

Fig. 2. Nitrogen adsorption–desorption isotherms obtained at 77 K and derived PSD for the HCMSC. Solid circle: adsorption, open circle: desorption.

Table 1
Surface structural parameters for the HCMSC and VC carbon black.

Sample	S_{BET} (m^2/g)	V_{total} (cc/g)	V_{meso} (cc/g)	V_{micro} (cc/g)	Pore size (nm)
HCMSC	1767	2.21	1.60	0.61	3.5
VC	235	0.32	0.22	0.10	–

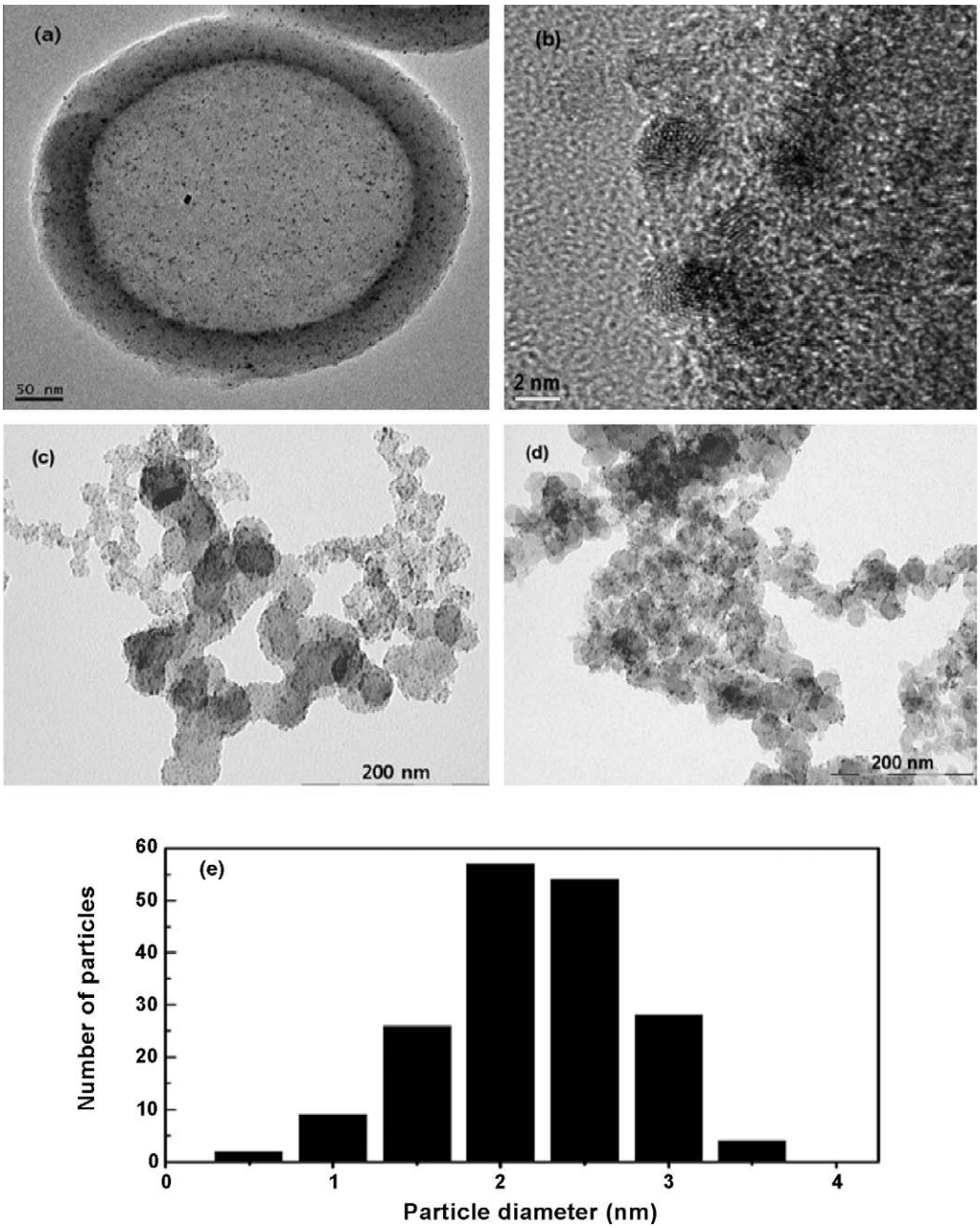

Fig. 3. HR-TEM images of PtRu (20 wt%)/HCMSC (a and b), TEM images of in-house PtRu (20 wt%)/VC (c) and commercial E-TEK PtRu (20 wt%)/VC (d), and PtRu particle size distribution diagram for the PtRu (20 wt%)/HCMSC (e).

directly from the HR-TEM image shown in Fig. 3a at randomly selected HCMSC-supported catalyst is ca. 2.2 nm with narrow size distribution of from 1.6 to 2.7 nm as shown in Fig. 3e. The HR-TEM image in Fig. 3b also shows small PtRu crystalline particles dispersed on the HCMSC matrix. In contrast, although most of the PtRu nanoparticles are dispersed homogenously on the VC support as shown in Fig. 3c (in-house made catalyst) and Fig. 3d (E-TEK one), Pt aggregation has been observed in certain areas. Furthermore, PtRu nanoparticles supported on the VC (in-house made catalyst) seem to have larger particle size compared with ones supported on the HCMSC.

Composition and nanoparticle size of the supported catalysts were examined by XRD analyses. Typical XRD patterns of the HCMSC or VC-supported PtRu (20 wt%) catalysts are shown in Fig. 4. All the supported PtRu catalysts exhibit XRD patterns typical of the Pt fcc structure. No peak was found to be related to tetragonal RuO_2 and hcp Ru phase, suggesting the presence of the Pt-Ru nanoparticles as an alloy. The average particle size of 2.3 nm was calculated for the HCMSC-supported PtRu nanoparticles from the Pt (2 2 0) reflection of the XRD patterns according to the Scherrer equation, which is close to that (2.2 nm) of the commercial E-TEK PtRu/VC and smaller than that (2.8 nm) of the in-house PtRu/VC. Uniformly dispersed PtRu alloy nanoparticles on the HCMSC support with smaller particle size were expected to provide good catalytic activity toward hydrogen electro-oxidation under the anode operation condition of PEMFC.

3.2. Electrochemical surface area and PEMFC polarization performance of various carbon-supported anode catalysts

Electrochemical surface area of Pt in a supported catalyst reflects the intrinsic electrocatalytic activity of the Pt-based

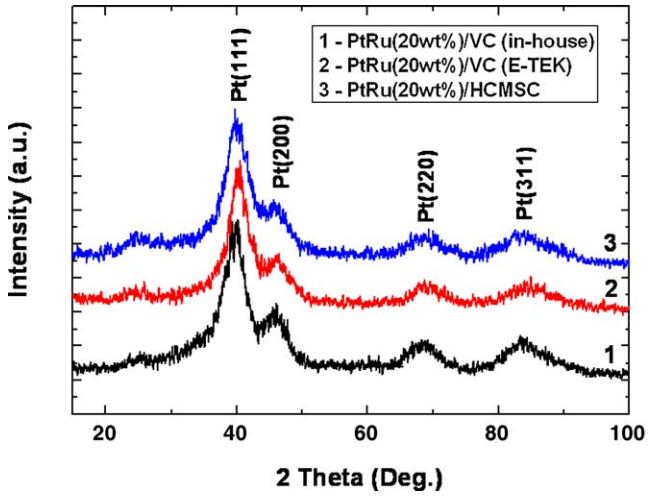

Fig. 4. Typical XRD patterns for the HCMSC- or the commercial carbon black VC-supported PtRu (20 wt%) catalysts.

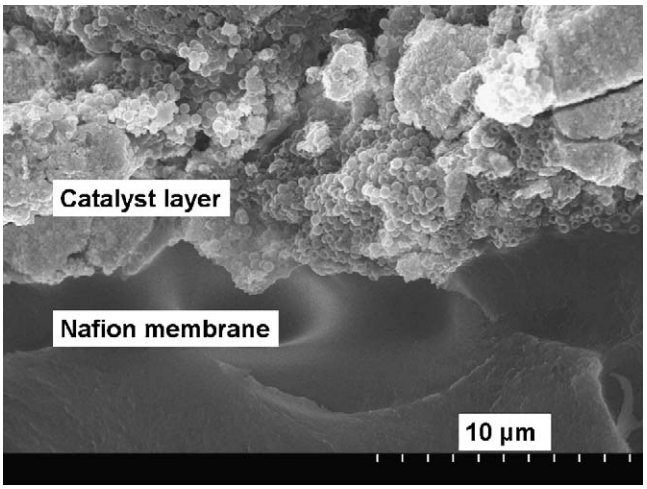

Fig. 6. SEM image of cross-section of the HCMSC-supported PtRu catalyst layer.

catalyst. This parameter can be obtained by the measurement of the steady-state cyclic voltammograms in a supporting electrolyte (i.e., 0.5 M H_2SO_4) followed by the determination of the integrated charge (after subtraction of capacitance contribution) in the hydrogen absorption region and the calculation based on a monolayer hydrogen adsorption charge of 0.21 mC/cm^2 on Pt polycrystalline. Fig. 5a shows representative CV curves at 25 mV/s for the VC or HCMSC-supported PtRu (20 wt%) catalysts in 0.5 M H_2SO_4. The well-known hydrogen adsorption–desorption characteristics were observed for all the carbon-supported PtRu catalysts. Electrochemical surface areas were calculated to be 85 m^2/g for Pt in the HCMSC-supported PtRu (20 wt%) catalyst, which is much larger than that (i.e., 51 m^2/g) for Pt in PtRu (20 wt%)/VC (in-house) and also larger than that (i.e., 63 m^2/g) for Pt in PtRu (20 wt%)/VC (E-TEK). Compared with the in-house VC-supported Pt catalyst, larger electrochemical surface area of Pt in the HCMSC-supported PtRu catalyst is mainly attributable to the smaller particle size and better dispersion of the Pt nanoparticles in the latter. Compared with the commercial VC-supported PtRu catalyst, larger electrochemical surface area of Pt in the HCMSC-supported PtRu catalyst is probably related to the better dispersion of the supported Pt nanoparticles and the unique hierarchical pore network of the HCMSC, facilitating mass transport.

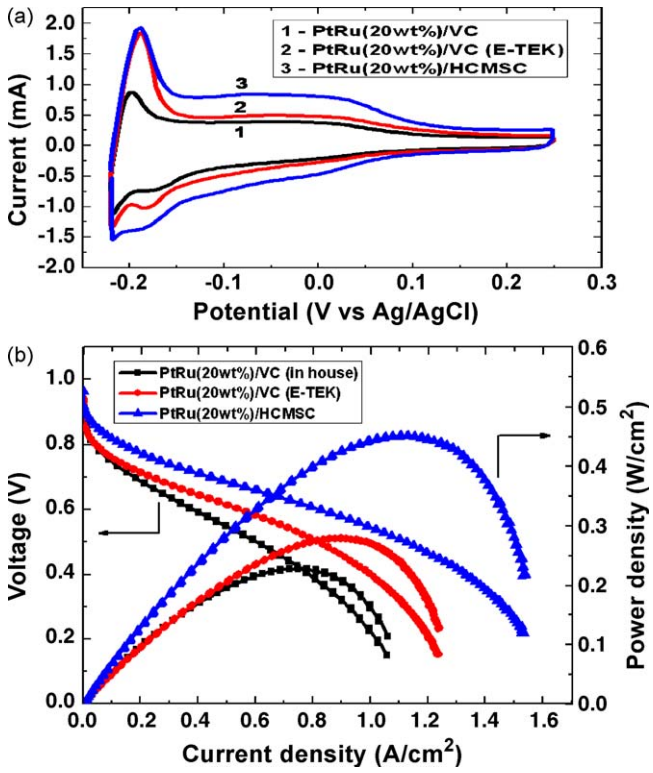

Fig. 5. Hydrogen electrosorption voltammetric profiles obtained in 0.5 M H_2SO_4 with a scan rate of 25 mV/s (a) and PEMFC polarization and power density plots at 60 °C for a single cell using various carbon-supported PtRu (20 wt%) anode catalysts for hydrogen oxidation (b).

Fig. 5b shows the polarization performance and power density plots for PEMFCs using various carbon-supported PtRu (20 wt%) anode catalysts at 60 °C. At low current density (i.e., less than 50 mA/cm^2), fuel cell polarization is mainly under electrochemical activation control. In this region, appreciably smaller electrochemical polarization was observed from the HCMSC-supported anode catalyst than the VC-supported ones, likely implying faster anodic hydrogen electro-oxidation kinetics on the surface of the former. Furthermore, the PtRu (20 wt%)/HCMSC catalyst exhibits a much higher maximum power density (i.e., 452 mW/cm^2) than that (i.e., 230 mW/cm^2) of the in-house PtRu (20 wt%)/VC and that (i.e., 279 mW/cm^2) of the PtRu (20 wt%)/VC (E-TEK) catalyst. This corresponds to an enhancement of 62% compared with that of the state-of-the-art E-TEK catalyst. It is worthwhile to note that the PtRu (20 wt%)/VC (in-house) catalyst prepared under the same condition as the PtRu (20 wt%)/HCMSC shows lower power density than that of the commercial PtRu (20 wt%)/VC (E-TEK) one, mainly resulting from the larger PtRu alloy nanoparticle size of the former catalyst. Although so, the PtRu/HCMSC catalyst has demonstrated considerably enhanced power density than the E-TEK one. Therefore, compared with the VC-supported PtRu anode catalysts, higher power density of the HCMSC-supported one should be attributed solely to the superb supporting effect of the HCMSC, related to its unique structural properties.

Larger specific surface area and mesoporous volume of the HCMSC enable the supported PtRu catalyst to have a more uniform dispersion of PtRu nanoparticles along with smaller nanoparticle size, resulting in more active reaction sites for the electro-oxidation of hydrogen. In addition, the well-developed bimodal nanoporous structure with the mesopores in the shell open to the outer surface and to the inner hollow macroporous core provides an open highway network around the active PtRu nanoparticles for fast mass transport. Furthermore, both the 3D interconnected large interstitial spaces between the packed spherical carbon particles

and the macroporous hollow core are open to the mesoporous channels in the shell, which can serve as the reservoirs of the reactants and products and shorten the diffusion path and facilitate mass transport. From the SEM image of cross-section of the interface between Nafion electrolyte and HCMSC-supported PtRu catalyst layer shown in Fig. 6, it was found that although the HCMSC-supported PtRu catalyst particles are in closely packed arrangement, there is large channel (space) in the catalyst layer due to the large particle size of the HCMSC with spherical morphology. In this case, the PtRu nanoparticles are not readily covered by the HCMSC support and likely exposed to the electrolyte, facilitating the access of the reactant into the catalyst layer and the removal of the product. In contrast, randomly distributed pores with varying sizes in the VC may make mass transport less efficient.

4. Conclusions

In this study, HCMSC has been investigated as an anode catalyst support in PEMFC. The HCMSC has possessed fantastic structural characteristics such as large specific surface area, mesoporous volume and well-developed 3D interconnected bimodal porosity composed of macroporosity of the hollow core and mesoporosity in the shell. Compared with the VC-supported PtRu catalysts, particularly in-house one, the HCMSC-supported catalyst has shown smaller PtRu nanoparticle size with better dispersion due to the superb structural characteristics of the HCMSC. The HCMSC-supported catalyst has exhibited great enhancement in the electrocatalytic activity toward hydrogen electro-oxidation and in fuel cell performance (with enhancement of more than 60% in power density compared with that of commercial E-TEK PtRu/VC), implying that the HCMSC is a potentially excellent anode catalyst support in PEMFC.

Acknowledgements

The authors thank KETEP and WCU Research Program for financial support and the Korean Basic Science Institute at Jeonju, Chuncheon and Deajeon for SEM, TEM and XRD measurements. In particular, JSYu thanks Prof. Vincenzo Tricoli at University of Pisa for helpful discussion regarding this work.

References

[1] N.A. Oliveira, E.G. Franco, E. Arico, M. Linardi, E.R. Gonzalez, J. Eur. Ceram. Soc. 23 (2003) 2987.
[2] R. Service, Science 296 (2002) 1222.
[3] S.B. Yoon, B. Fang, M. Kim, J.H. Kim, J.-S. Yu, in: G. Wilde (Ed.), Nanostructured Materials, Elsevier, 2009, pp. 173–231 (Chapter 4).
[4] H.C. Yu, K.Z. Fung, T.C. Guo, W.L. Chang, Electrochim. Acta 50 (2004) 807.
[5] J.R.C. Salgado, E. Antolini, E.R. Gonzalez, J. Phys. Chem. B 108 (2004) 17767.
[6] U.A. Paulus, A. Wokaun, G.G. Scherer, T.J. Schmidt, V. Stamenkovic, V. Radmilovic, N.M. Markovic, P.N. Ross, J. Phys. Chem. B 106 (2002) 4181.
[7] E. Casado-Rivera, D.J. Volpe, L. Alden, C. Lind, C. Downie, T. Vazquez-Alvarez, A.C.D. Angelo, F.J. DiSalvo, H.D. Abruna, J. Am. Chem. Soc. 126 (2004) 4043.
[8] Â.N.M. Markovic, T.J. Schmidt, V. StamenkovicÂ, P.N. Ross, Fuel Cells 1 (2001) 105.
[9] G.-Y. Chen, D.A. Delafuente, S. Sarangapani, T.E. Mallouk, Catal. Today 67 (2001) 341.
[10] S.-J. Liao, K.-A. Holmes, H. Tsaprailis, V.I. Birss, J. Am. Chem. Soc. 128 (2006) 3504.
[11] C. Rice, S. Ha, R.I. Masel, A. Wieckowski, J. Power Sources 115 (2003) 229.
[12] H.A. Gasteiger, N. Markovic, NJrR. Philip, E. Cairns, J. Electrochim. Acta 39 (1994) 1825.
[13] Y.Y. Tong, H.S. Kim, P.K. Babu, P. Waszczuk, A. Wieckowsk, E. Oldfield, J. Am. Chem. Soc. 124 (2002) 468.
[14] J. Luo, P.N. Njoki, Y. Lin, L.-Y. Wang, C.-J. Zhong, Electrochem. Commun. 8 (2006) 581.
[15] D.C. Papageorgopoulos, M. Keijzer, J.B.J. Veldhuis, F.A. de Bruijn, J. Electrochem. Soc. 149 (2002) A1400.
[16] J.L. Fernandez, D.A. Walsh, A.J. Bard, J. Am. Chem. Soc. 127 (2005) 357.
[17] V. Raghuveer, P.J. Ferreira, A. Manthiram, Electrochem. Commun. 8 (2006) 807.
[18] Z.-Q. Tian, S.-P. Jiang, Y.-M. Liang, P.-K. Shen, J. Phys. Chem. B 110 (2006) 5343.
[19] C. Wang, M. Waje, X. Wang, J.M. Tang, R.C. Haddon, Y. Yan, Nano Lett. 4 (2004) 345.
[20] E.S. Steigerwalt, G.A. Deluga, D.E. Cliffel, C.M. Lukehart, J. Phys. Chem. B 105 (2001) 8097.
[21] F. Su, J. Zeng, X. Bao, Y. Yu, J.Y. Lee, X.S. Zhao, Chem. Mater. 17 (2005) 3960.
[22] J. Ding, K.Y. Chan, J. Ren, F.S. Xiao, Electrochim. Acta 50 (2005) 3131.
[23] G.-S. Chai, S.-B. Yoon, J.-S. Yu, Carbon 43 (2005) 3028.
[24] B. Fang, J.H. Kim, J.-S. Yu, Electrochem. Commun. 10 (2008) 659.
[25] C. Vix-Guterl, E. Frackowiak, K. Jurewicz, M. Friebe, J. Parmentier, F. Béguin, Carbon 43 (2005) 1293.
[26] B. Fang, M. Kim, S. Hwang, J.-S. Yu, Carbon 46 (2008) 876.
[27] G.S. Chai, S.B. Yoon, J.-S. Yu, J.-H. Choi, Y.-E. Sung, J. Phys. Chem. B 108 (2004) 7074.
[28] F. Su, X.-S. Zhao, Y. Wang, J. Zeng, Z. Zhou, J.-Y. Lee, J. Phys. Chem. B 109 (2005) 20200.
[29] G.-S. Chai, I.-S. Shin, J.-S. Yu, Adv. Mater. 16 (2004) 2057.
[30] Y.-C. Liu, X.-P. Qiu, Y.-Q. Huang, W.-T. Zhu, G.-S. Wu, J. Appl. Electrochem. 32 (2002) 1279.
[31] M. Kim, S. Hwang, J.-S. Yu, J. Mater. Chem. 17 (2007) 1656.
[32] H. Wu, J.-G. Chen, J. Vac. Sci. Technol. A 21 (2003) 148.
[33] J.-H. Dong, Y.-K. Kim, S.-H. Han, J.-S. Lee, Catal. Today 132 (2008) 117.
[34] S.B. Yoon, K. Sohn, J.-Y. Kim, C.-H. Shin, J.-S. Yu, T. Hyeon, Adv. Mater. 14 (2002) 19.
[35] G.S. Chai, S.-B. Yoon, J.-H. Kim, J.-S. Yu, Chem. Commun. 23 (2004) 2766.
[36] J.Y. Kim, S.J. Lee, J.-S. Yu, Bull. Korean Chem. Soc. 21 (2000) 544.
[37] B. Fang, M. Kim, J.-S. Yu, Appl. Catal. B: Environ. 84 (2008) 100.